Biomacromolecules

pubs.acs.org/Biomac

Article

NIR Light-Mediated Photocuring of Adhesive Hydrogels for Noninvasive Tissue Repair *via* Upconversion Optogenesis

Peyman Karami,[§] Vijay Kumar Rana,[§] Qianyi Zhang,[§] Antoine Boniface, Yanheng Guo, Christophe Moser, and Dominique P. Pioletti*

Cite This: *Biomacromolecules* 2022, 23, 5007−5017

Read Online

ACCESS | Metrics & More | Article Recommendations | Supporting Information

ABSTRACT: The surgical treatments of injured soft tissues lead to further injury due to the use of sutures or the surgical routes, which need to be large enough to insert biomaterials for repair. In contrast, the use of low viscosity photopolymerizable hydrogels that can be inserted with thin needles represents a less traumatic treatment and would therefore reduce the severity of iatrogenic injury. However, the delivery of light to solidify the inserted hydrogel precursor requires a direct access to it, which is mostly invasive. To circumvent this limitation, we investigate the approach of curing the hydrogel located behind biological tissues by sending near-infrared (NIR) light through the latter, as this spectral region has the largest transmittance in biological tissues. Upconverting nanoparticles (UCNPs) are incorporated in the hydrogel precursor to convert NIR transmitted through the tissues into blue light to trigger the photopolymerization. We investigated the photopolymerization process of an adhesive hydrogel placed behind a soft tissue. Bulk polymerization was achieved with local radiation of the adhesive hydrogel through a focused light system. Thus, unlike the common methods for uniform illumination, adhesion formation was achieved with local micrometer-sized radiation of the bulky hydrogel through a gradient photopolymerization phenomenon. Nanoindentation and upright microscope analysis confirmed that the proposed approach for indirect curing of hydrogels below the tissue is a gradient photopolymerization phenomenon. Moreover, we found that the hydrogel mechanical and adhesive properties can be modulated by playing with different parameters of the system such as the NIR light power and the UCNP concentration. The proposed photopolymerization of adhesive hydrogels below the tissue opens the prospect of a minimally invasive surgical treatment of injured soft tissues.

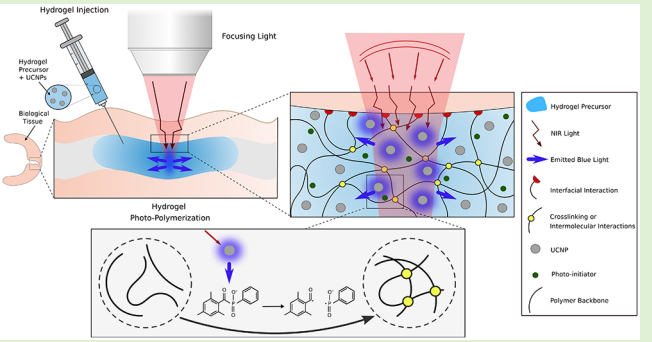

INTRODUCTION

The treatment of injured soft tissues or arteries is typically done by arthroscopy. For instance, suturing a torn meniscus often requires centimeter-scale incisions on the knee and creating holes in the healthy meniscus through complex invasive suturing techniques.[1] Incisions are ubiquitous for repairing internal bleeding due to ruptured arteries.[2] These procedures are traumatic and challenging, which can potentially result in the damage of surrounding tissues, creating what is called an iatrogenic injury. The esthetic aspects of postsurgery healing are equally crucial and need attention.

A potential alternative method to sutures, for the treatment of such torn soft tissues, has been shown by using bioadhesive materials, although with limited success.[3] The bioadhesive material is brought deep inside biological tissues by a minimally invasive technique. Among various types of cross-linking (*e.g.*, enzymatic, thermal, chemical, physical, *etc.*), light-responsive biomaterials (*e.g.*, photocurable hydrogels) constitute an interesting class of biomaterials for clinical situations because the light, as opposed to other stimuli, can be remotely applied and tuned to activate the biomaterial *in situ*. Therefore, it provides the distinct advantages of precise three-dimensional (3D) control of polymerization.[4] Owing to a native extracellular matrix (ECM), hydrogels, which are water-swollen polymer 3D networks, are of utmost interest in biomedical fields since they permit the encapsulation of cells and can be engineered with a plethora of biological signals.[3,5,6]

The design of photocurable hydrogels presenting sufficient injectability *via* a thin cannula, adhesion, and physicochemical properties is demanding.[7,8] A variety of techniques have been established to develop hydrogels for biomedical applications. However, the light-triggered curing of the bioadhesives highly

Received: June 30, 2022
Revised: November 1, 2022
Published: November 15, 2022

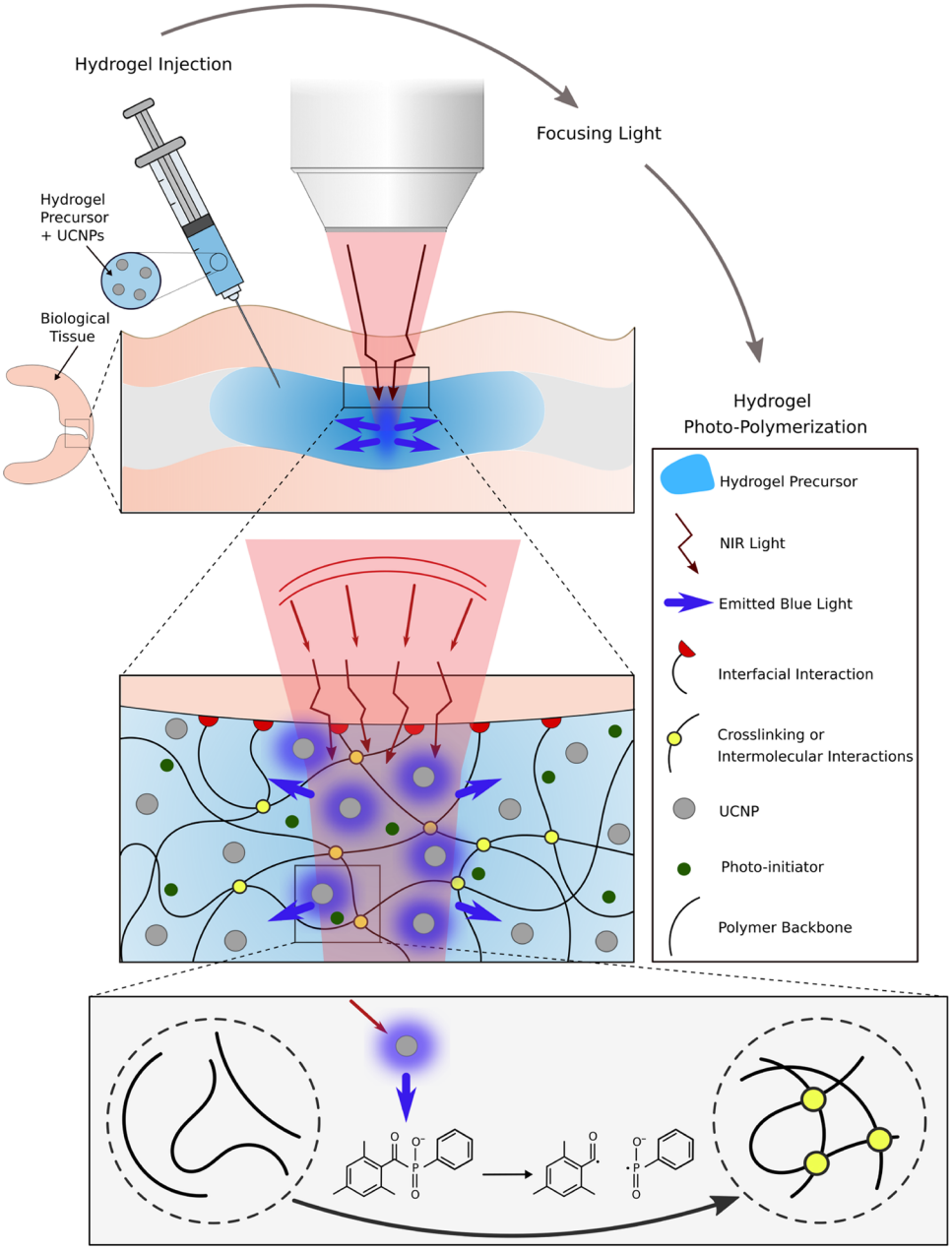

Figure 1. Schematic of NIR light-mediated photocuring of an adhesive hydrogel below the tissue. The UCNP-containing hydrogel precursor is first injected through the tissue. NIR interacts and activates UCNPs. Due to light scattering by the tissue, the focused radiation system shapes the incident NIR and maximizes the transmitted intensity. Subsequently, the photopolymerization occurs through emission of blue light by UCNPs and in the presence of a photoinitiator. The photoinitiator absorbs the upconverted photons and upon excitation, produces radicals that initiate polymerization of MePGa-Gel and induces the cross-linking between the polymer chains.

relies on using the high-energy short-wavelength light to induce photopolymerization. Conventionally, hydrogels are fabricated by embedding photoinitiators in a hydrogel precursor, which are then activated with ultraviolet (UV) or blue light. This method can be noninvasive as long as UV/visible light propagates through biological tissues. However, in addition to the serious biosafety concerns and adverse biological effects of short-wavelength lights on tissue, the short penetration depth of blue/visible wavelength into tissue is not appropriate to cure adhesive hydrogels deep inside biological tissues.[9] In some reported hydrogel systems, the photopolymerization can also be performed with the green light; however, they can present some concerns regarding using commercial and biocompatible photoinitiators, as well as the light penetration depth.[10]

Biological tissues are optically complex turbid media. Light transport in such media is governed by their absorption and scattering properties.[11,12] Near-infrared light (NIR) ranging from 650 to 1350 nm, also known as the spectral optical window, allows a greater depth penetration in tissue due to reduced absorption and scattering than shorter wavelengths in the visible or UV spectrum.[13−15] NIR has also lower energy per photon, which limits potential damage to biomolecules in cells and tissues.[13,16] This is why, these wavelengths (NIR) are exploited to visualize tissue morphology and physiology at cellular level deep within scattering tissue by two/three-photon

https://doi.org/10.1021/acs.biomac.2c00811
Biomacromolecules 2022, 23, 5007−5017

microscopy.[17,18] Therefore, to circumvent the limited penetration of UV/visible light, NIR can be used to increase penetration depth and thanks to upconverting nanoparticles (UCNPs) dispersed into the hydrogels, photopolymerization can be triggered by the local generation of blue light created by multiphoton absorption of the NIR light.

Lanthanide ions in UCNPs have the capability of photon upconversion through a mechanism, in which multiple low-energy photons are used to excite an electron to a high energy level which generates a single high-energy photon. In lanthanide-doped upconversion nanoparticles, the ladder-like electronic energy structure of lanthanides can be exploited to precisely tune the emission of UCNPs to a particular wavelength by controlling the energy transfer *via* selective lanthanide-ion doping.[19,20] UCNPs composed of a $NaYF_4$ ceramic host codoped with Yb^{3+} as a sensitizer and Er^{3+} or Tm^{3+} as an activator are considered as one of the efficient anti-Stokes photoluminescent materials.[21] These materials can generate shorter wavelength photons (in the UV/blue) from two or more longer wavelength photons (in the NIR). Recently, the triplet−triplet annihilation (TTA) process has also been employed for the development of UCNPs with enhanced upconversion efficiency, while a low excitation power is required. In optical triplet−triplet annihilation upconversion (TTA-UC), long wavelength photons with low energy can be converted to shorter wavelength photons to provide high power.[22,23] This is of high interest particularly in biomedical applications, in which safe doses of irradiation is a significant consideration.

UCNPs have been widely used in upconversion luminescence, biosensing, high-contrast bioimaging, photoacoustic imaging, photodynamic therapy, and other disease treatment.[21,24,25] Recently, however, Chen et al. used UCNPs for 3D printing technology that enables the noninvasive *in vivo* 3D bioprinting of tissue constructs,[24] whereas Chen et al. employed UCNPs as optogenetic actuators of NIR light to stimulate deep brain neurons.[26] Curing adhesive hydrogels deep below the tissue for the treatment of torn soft tissues through a focused light system without incisions has not been proposed early where UCNPs are employed to trigger photopolymerization using NIR light.

In this study, we report on how NIR can be used to form adhesive hydrogels through biological tissues without incisions, leading to a potentially alternative method to treat torn soft tissues (see Figure 1). With a local radiation of the adhesive hydrogel precursor, through a focused beam of NIR light with adjustable power, we proposed a tunable and nonlinear bulk photopolymerization. This is achieved, thanks to $NaYF_4$/Yb,Tm UCNPs homogeneously dispersed in the precursor of the hydrogel that allow to convert NIR light into UV/blue photons. The isotropically emitted blue light initiates the photopolymerization of the precursor (phosphoserine-modified methacryloyl gelatin, MePGa-Gel)[7] after the activation of a widely used and commercially available photoinitiator (lithium phenyl-2,4,6-trimethyl-benzoyl phosphinate, LAP). Consequently, the hydrogel network is formed through chemical reactions between polymer chains, while the hydrogel adheres to the tissue with its interfacial bonds. Indeed, LAP is known for its cytocompatibility and is used broadly in biomedical applications.[27] MePGa-Gel is used for creating interfacial interactions with biological tissues. We performed a series of experiments with changing either the thickness of the tissues or the composition of the gel and showed that NIR is an excellent alternative to UV to polymerize adhesive hydrogels located below and inside tissues and as well to avoid the detrimental damages by UV exposure.

MATERIALS AND METHODS

Synthesis of $NaYF_4$/Yb,Tm Core−Shell Particles. The synthesis of UCNPs was performed using a method reported earlier.[24,26] Briefly, the core of UCNPs was synthesized by adding $YCl_3{\cdot}6H_2O$ (168.67 mg, 0.556 mmol), $YbCl_3{\cdot}6H_2O$ (93.00 mg, 0.24 mmol), and $TmCl_3$ (1.1 mg, 0.004 mmol) to a 100 mL flask containing 6 mL of oleic acid and 14 mL of 1-octadecene. The solution was heated to 140 °C under vacuum for 1 h to obtain a homogeneous transparent light-yellow solution. Once the solution was cooled, 10 mL of methanol solution of NH_4F (118.50 mg, 3.2 mmol) and NaOH (80 mg, 2 mmol) was added. The resulting cloudy mixture was stirred for another 30−45 min at 50 °C. Subsequently, the methanol was distilled off after heating at 120 °C for 1 h. After three rounds of N_2 purging at 120 °C, the solution was heated to 300 °C quickly under the N_2/Ar flow and kept for 1.5 h. The mixture was precipitated by the addition of 20 mL of ethanol and collected by centrifugation at 4000 rpm for 3 min. After washing four times in ethanol, the final product $NaYF_4$/Yb,Tm was redispersed in 4 mL of cyclohexane.

To suppress surface quenching causing luminescence weakening, an optically inert shell layer of NaY_4F was grown epitaxially onto the as-synthesized UCNPs. Specifically, 0.8 mmol of $YCl_3{\cdot}6H_2O$ (242.69 mg) was mixed with 6 mL of oleic acid and 14 mL of 1-octadecene and heated at 150 °C for 1.5 h. After cooling to 80 °C, all of the UCNP products ($NaYF_4$/Yb,Tm) from the previous step (in 4 mL of cyclohexane) were added to the reaction mixture. The solution was further stirred at 80 °C for 1 h to evaporate the cyclohexane content. Subsequently, a methanol solution containing 2 mmol of NaOH (80 mg) and 3.2 mmol of NH_4F (118.50 mg) was added to the reaction solution at 50 °C. After 0.5 h of continuous stirring at 50 °C, the reaction was heated to 120 °C under vacuum for 1 h. After three rounds of N_2 purging at 120 °C, the reaction temperature was ramped to 300 °C and maintained at 300 °C for 1.5 h. The reaction was cooled down to room temperature, and the core−shell UCNP products were washed twice with ethanol and dispersed into 4 mL of cyclohexane.

The as-synthesized UCNPs were transferred into an aqueous phase through an acid-induced ligand removal process. Cyclohexane (4 mL) was added with 4 mL of ethanol and centrifuged at 5000 rpm for 3 min. The pellet was redispersed with a mixture of 4 mL of ethanol and 4 mL of HCl aqueous solution (2 M) by sonication. The acid-treated UCNPs were thereafter washed three times with ethanol to remove excess acid content. The ligand-free UCNPs were dispersed into 4 mL of deionized (DI) H_2O for subsequent surface modification.

Tissue Preparation. To evaluate the effect of tissue thickness on the NIR light transmission and hydrogel photopolymerization, we prepared tissues with various thicknesses. The tissue samples were prepared from fresh articular cartilage isolated from bovine knee. Accordingly, we first cut cartilage-on-bone blocks from the femoropatellar groove in small sizes. Afterward, the tissue blocks were embedded in 5 wt % agarose (Sigma-Aldrich, A9539) solution and solidified in an ice container. Tissue blocks were then mounted (glued) onto the cutting stage in cold phosphate-buffered saline (PBS) shortly after fixation and sliced into tissue sections with a defined thickness using a vibratome. To have a precise comparison between samples with different thicknesses, all tissue pieces were cut from the top part of the cartilage layer, so that the thicker samples were just obtained with a deeper cut, including the superficial zone. The tissue samples were sliced into 100−800 μm thick sections and then collected in PBS for the analysis.

Hydrogel Synthesis. The adhesive gelatin-based hydrogel was fabricated on the basis of our previously published protocol.[7] MePGa polymers were synthesized using a two-step modification process including (i) methacrylation of the gelatin backbone and (ii) phosphoserine functionalization. Briefly, 5 g of gelatin type A from porcine skin (G2500, Sigma-Aldrich) was dissolved in 50 mL of

https://doi.org/10.1021/acs.biomac.2c00811
Biomacromolecules 2022, 23, 5007−5017

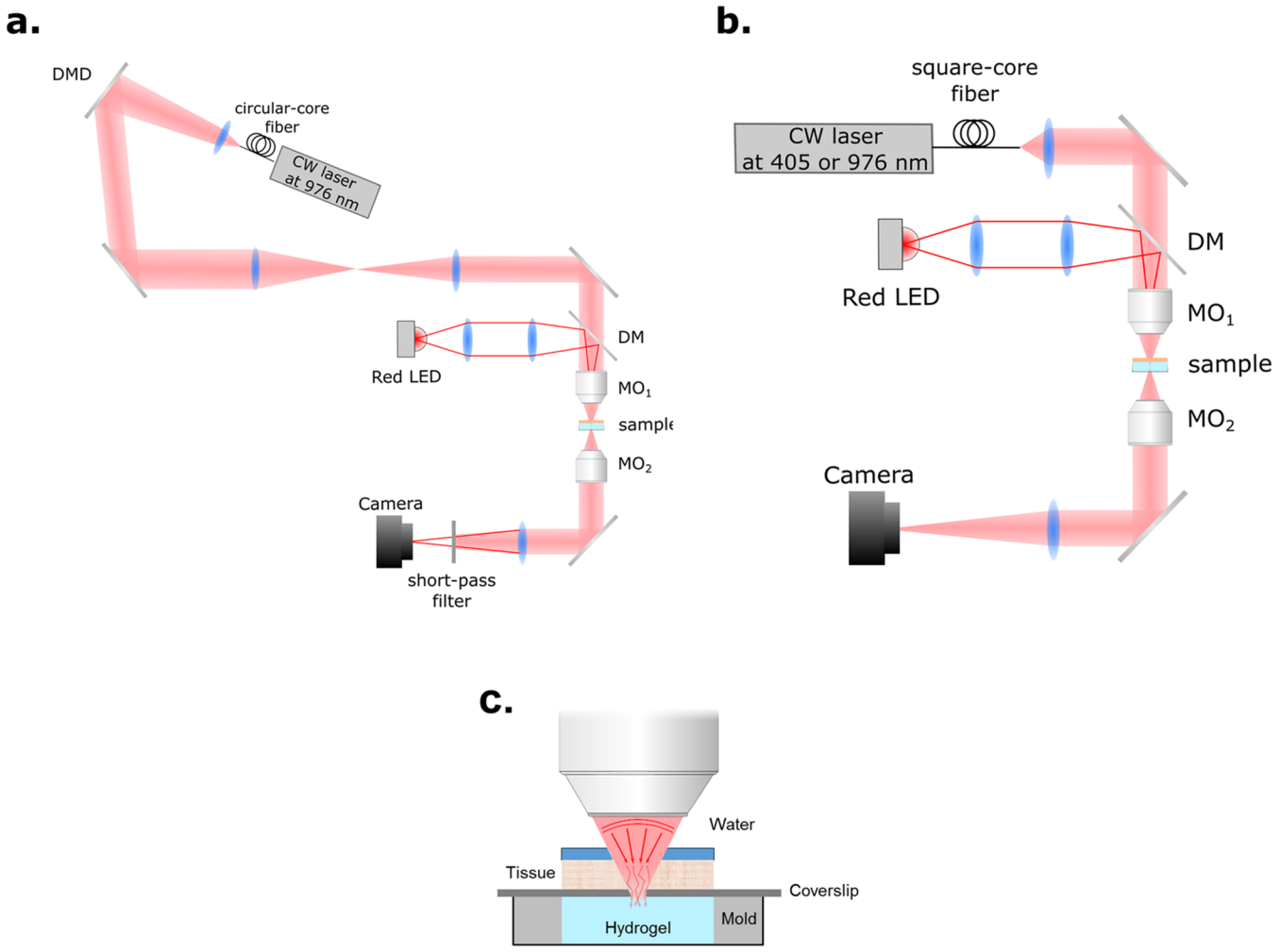

Figure 2. Experimental setup (a) for photopolymerization with NIR and (b) transmission measurement. (c) Schematic of sample preparation for the optical setup.

Dulbecco's phosphate-buffered saline (DPBS) and heated at 60 °C for 30 min. Subsequently, 3 mL of methacrylic anhydride (276685, Sigma-Aldrich) was added dropwise to the solution. After 2 h of continuous stirring, the solution was diluted 5 times and dialyzed against distilled water at 50 °C for 5 days. The lyophilization of the solution was then performed for 4 days to obtain the resulting methacrylated polymer. The second modification step was carried out by dissolving 1 g of the methacrylated gelatin in 50 mL of MES buffer at the pH of 5. Following EDC/NHS activation of the solution at 37 °C for 15 min, phosphoserine (17885-08-4, Flamma) was added (25 mM). The mixture was stirred vigorously for 8 h, dialyzed for 5 days, and lyophilized for 4 days to obtain the MePGa product.

The hydrogel precursor was synthesized by dissolving the produced MePGa polymer in distilled water. The resulting solution was then mixed with the LAP photoinitiator (6146, Tocris Bioscience) and the UCNP solution. The final concentration of MePGa and LAP in the precursor was 15 and 0.2 wt %, respectively. The resulting solution was well mixed by vortexing and sonication for at least 15 min to have homogeneous distribution of the particles. To improve the efficacy of the UCNPs for radical polymerization in hydrogels, the UCNPs were coated with the LAP photoinitiator by sonication of their mixture for 1 h before mixing with the MePGa polymer.

Dynamic Light Scattering. To characterize the photoinitiator coating on the UCNPs, ζ-potential (ZP) measurements were performed on a Malvern Zetasizer NS90 instrument. The ζ-potential was measured after diluting all of the samples 10-fold.

Optical Setup for Photopolymerization and Transmission Measurement. A continuous-wave (CW) laser at 976 nm (9 W, LU09xxT090, Lumics) is coupled into a multimode circular-core fiber (NA 0.22, 105 μm). The output beam is collimated by a lens (F230APC-980, Thorlabs, f = 4.55 mm) and modulated (amplitude-only modulation) by a digital micromirror device (DMD) (V-650L, Vialux). The angle of incidence is ~17° relative to the surface normal of the DMD, giving a maximal efficiency for a reflection angle of ~41°. The diffraction efficiency in this configuration is 50%. In this experiment, all of the micromirrors are set to the "on" state, making the DMD a pure mirror. After that, the plane of the DMD is relayed by a 4-f system made of two lenses (f = 300 mm) to the back aperture of a microscope objective MO_1 (20×, NA 0.40, WD 20 mm, Mitutoyo). The latter focuses the NIR light on the sample. The focal plane is imaged by a second objective MO_2 (10×, NA 0.25 Leica) onto a camera (BFS-U3-31S4M-C, FLIR) for passive monitoring. The tube lens has a focal length f = 100 mm, leading to an effective magnification of 5. A red light-emitting diode (LED) is used as an illumination source for bright-field imaging. The red light propagates through a 4-f system made of a microscope objective (4×, NA 0.13, Olympus), and a lens (f = 75 mm) is merged with the NIR laser by a long-pass dichroic mirror and projects onto the MO_1 back aperture. Bright, uniform illumination with a diameter of 1.4 mm is created on the focal plane of MO_1 (see Figure 2a).

The measurement of the transmission of 405 and 976 nm light requires that both lights propagate in the same way. Therefore, the configuration of the NIR laser before MO_1 is replaced by a fiber. Both laser sources are coupled into the same multimode square fiber (NA 0.22, 200 μm, CeramOptec). This fiber has FC/APC connectors that can be mounted and unmounted easily with good repeatability. The

https://doi.org/10.1021/acs.biomac.2c00811
Biomacromolecules 2022, 23, 5007−5017

output of the square fiber is collimated by a lens (f = 10 mm) and focused by MO_1. The rest of the setup is the same as that of the photopolymerization (see Figure 2b).

Sample Preparation. The sample consists of a hydrogel in a reservoir with a layer of biological tissue on top with a controlled thickness. We also studied the case with no tissue as a reference sample. The hydrogel is injected in the cylindrical mold without upper and lower surfaces. The mold has a height of 2 mm and a diameter of 5 mm. The bottom is sealed by transparent tape to minimize the light reflection and improve imaging. A coverslip is placed onto the mold, and the tissue is placed on top with a droplet of phosphate-buffered saline to keep the tissue in good conditions (see Figure 2c).

Sample Alignment. The position of the mold is adjusted based on bright-field imaging. First, the focus knob on the mechanical stage is calibrated by the z-axis translation mount of MO_2, which has a known travel distance. Next, the mold sealed with transparent tape is placed on the mechanical stage and the focus knob is adjusted to sharpen the focus quality of the image of the tape. Then, the stage is lowered by the knob to 1.3 mm to ensure that the imaging plane is inside the gel. Finally, the NIR laser is turned on at low intensity and the z-position of MO_1 is adjusted to get the smallest focal spot on the imaging plane.

Transmission Measurement. To avoid any chemical reaction (induced photopolymerization) in this measurement, the mold is filled with gelatin solution (15% w/v), which has the same optical property as the precursor for photopolymerization in this study. The sample is prepared and aligned on the stage, and the NIR light is set to fixed power. The z-position of MO_1 is adjusted to find the smallest speckle, which is viewed and recorded on the camera. The speckle pattern of the sample without cartilage on top is set as the reference. Then, the squared fiber is coupled to the UV source and the same steps are performed. For each sample, 20 positions in the gel are chosen randomly to measure the transmitted speckle pattern. The transmission and the normalized intensity are calculated based on the reference.

$$\text{transmission} = \frac{\text{sum of the speckle}}{\text{sum of the reference speckle}} \times 100\%$$

$$\text{normalized intensity} = \frac{\frac{\text{sum of the speckle}}{\text{area of the speckle}}}{\frac{\text{sum of the reference speckle}}{\text{area of the reference speckle}}} \times 100\%$$

Photopolymerization. After the preparation and alignment of the sample, the laser power is measured before MO_1 and tuned to a specific value, and photopolymerization begins. A short-pass filter is added before the camera to observe the change of the precursor. 10 min later, the NIR laser is turned off and the polymerized part sticking to the coverslip is taken out of the mold and kept in a humid environment for further characterization.

We compared the performance of the proposed NIR-mediated polymerization technique with that of a conventional UV/blue polymerization system with a uniform light distribution, consisting of a lamp of wavelength 405 nm with an intensity of 2 mW/cm^2. We used tissue samples of different thicknesses, and our hydrogel system was placed behind them. To measure the light power and its uniform distribution incident and transmitted through the tissue, we used a digital optical power and energy meter console (PM100D, Thorlabs) and obtained the light parameters in the location of the illuminating samples at the defined distance from the lamp. Furthermore, in addition to the uniform radial light distribution, the light intensity was measured along the z-axis to confirm the uniform light distribution throughout the bulk sample, in which no significant difference in intensity was observed between the top and bottom of the hydrogel precursor in its cylindrical mold, indicating a low scattering effect.

Scanning Electron Microscopy. Scanning electron microscopy (SEM) images of freeze-dried hydrogel samples were recorded using the InLens detector of GEMINI SEM 300 (Carl Zeiss Germany) at an acceleration voltage of 3 kV. The samples were placed on a dual-sided carbon tape stuck to a holder and coated by a 15 nm gold thin film before the analysis.

Transmission Electron Microscopy. Transmission electron microscopy (TEM) images were measured of UCNPs using a Thermo Fisher Tecnai-Spirit microscope operating at 120 kV. The samples were placed on a carbon grid and plotted with filter paper after 30 s. The sample was allowed to dry in air before the analysis.

Mechanical Characterization. *Nanoindentation.* To analyze the gradient mechanical properties of hydrogels below tissue, photopolymerized samples with different UCNP concentrations of 10, 15, and 20 mg/mL were characterized using a nanoindentation technique. The measurements were conducted using an Anton Paar tester (NHT^3) with a Berkovich diamond indenter tip. The cylindrical-shaped hydrogels were indented on the top face from the center to the edge at three different locations, and the corresponding local mechanical response is recorded at the radii of 0.1 R, 0.5 R, and 0.9 R from the cylinder axis. All tests are performed in wet conditions to avoid drying of the sample during measurement. During the indentation, a depth control mode with a maximum indentation depth of 20 μm was applied at a displacement rate of 10 μm/min. The maximum indentation force during the loading–unloading was reported.

Adhesion Measurement. The adhesive strength of the hydrogels was evaluated under tensile mode using an Instron E3000 linear mechanical testing machine (Norwood, MA) equipped by a 50 N load cell. The hydrogel precursor was injected inside cylindrical Teflon molds with 2 mm in height and 5 mm in diameter, and the host surface was placed on the top of the sample. Subsequently the hydrogel was photopolymerized using the optical setup and attached to the surface in contact. To have the same surface composition, we used a gelatin-coated glass substrate for the host surface, which was gripped in the adhesion setup after polymerization. The hydrogel was also fastened to the other Instron's grip, and the tensile load was applied with a constant loading rate of 0.1 mm/s. The adhesion strength was reported by dividing the maximum load to the overlap area (n = 3). We selected this evaluation method as the focal spot can be well adjusted inside the hydrogel in this test and reproducible measurements can be performed.

Compression Test. Cylindrical hydrogel samples were compressed using the Instron at a rate of 0.1 mm/s in PBS bath. Hydrogels were tested at different UCNP concentrations of 10, 15, and 20 mg/mL and NIR laser powers of 0.5, 0.7, and 0.9 W. The applied load and compressive strain were recorded and the compressive modulus of the hydrogels was calculated by linear interpolation of the stress–strain curve between 15–25% of strain (mm/mm) (n = 3).

Cytotoxicity Evaluation. *In vitro* cytocompatibility of the developed hydrogels was assessed in accordance with ISO 10993-5 standard, in which the fluid extract of the test samples were applied to the cultured cells. Briefly, bovine chondrocytes were incubated to near confluence in standard culture medium, supplemented with fetal bovine serum (10 vol %), penicillin-streptomycin (1 vol %), and L-glutamine (1 vol %), at 37 °C in 5% CO_2. To obtain the fluid extracts, the hydrogel samples were placed in a separate culture medium (ratio of sample surface area to medium volume: 2 cm^2/mL) and incubated at 37 °C for 24 h. Culture medium incubated at 37 °C without test samples was also used as a negative control. The cultured cells were seeded on a 96-well plate for 24 h, while each well contained 150 μL of culture medium at a concentration of 10^4cells/cm^2. Afterward, the culture medium was replaced with corresponding extracts derived from the test samples. The same procedure was followed for the negative control (n = 4). After 48 h exposure to the extracts, the cell viability was then assessed by a PrestoBlue cell viability reagent (A13261, Invitrogen) based on the manufacturer protocol. Accordingly, the medium was aspirated at the end of incubation and replaced with the medium containing 10 vol % PrestoBlue, followed by incubation at 37 °C for 30 min. Subsequently, the fluorescence intensity of the measurement medium was quantified at 595 nm using a microplate reader (Wallac 1420 Victor2, PerkinElmer). The cell viability was obtained based on the measured absorbance values and calculated as the percentage of absorbance in the control group (100% viability). Furthermore, cell viability analysis was assessed using a Live/Dead Assay Kit (Biotium, Fremont, CA) based on the

https://doi.org/10.1021/acs.biomac.2c00811
Biomacromolecules 2022, 23, 5007–5017

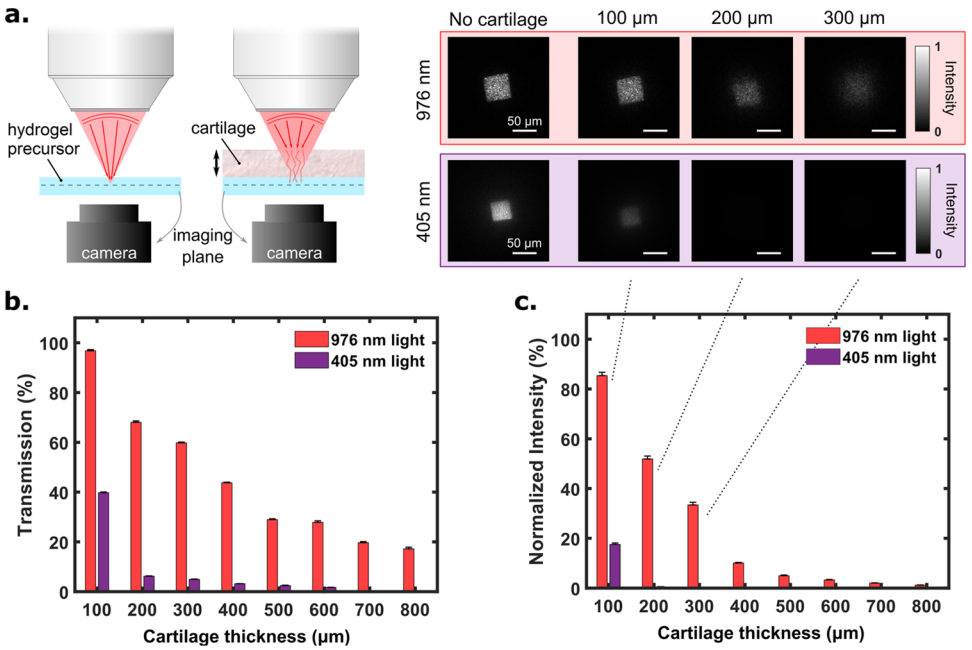

Figure 3. Comparison between 976 and 405 nm wavelength light for penetration depth through the bovine knee cartilage. (a, left hand side) Schematic view of the experimental setup. Light (blue or NIR), at the output of a square optical fiber, is focused through the tissue on the hydrogel (containing 15 wt % gelatin solution) with a microscope objective (magnification: 20×, numerical aperture: 0.4, working distance: 20 mm). (a, right hand side) Corresponding images taken with the camera for different tissue thicknesses at the focal plane of the microscope objective. From these measurements, both (b) transmission and (c) normalized intensity (normalized by "No Tissue") are plotted as a function of the tissue thickness.

manufacturer instruction. The live/dead staining solution was prepared by adding calcein AM and ethidium homodimer to PBS at 0.2 and 0.4 μL/mL concentration, respectively. The cells were incubated in the staining solution for 20 min protected from light. The live and dead cells were analyzed under an invert LSM 700 confocal microscope (Carl Zeiss, Jena, Germany) by taking florescence images at wavelengths adjusted for green and red dyes (see Supporting Figure 3).

RESULTS AND DISCUSSION

Although NIR is transmitted more efficiently through the tissue than blue and visible light, light scattering prevents focusing the light to a small spot. This effect reduces the light intensity below the tissue, and thus, there exists a threshold excitation intensity, which must reach to initiate the polymerization in a defined time period.

We first compare the transmission of NIR (976 nm) and blue light (405 nm) through the same tissue (cartilage) of different thicknesses (Figure 3a). We observed that transmission of the blue light is less than 10% in 200 μm tissue thickness, while that of NIR is still around 25% with 800 μm thickness (Figure 3b). The penetration depth of NIR is even more evident when looking at the transmitted intensity, which is the transmitted power per unit area and is a key parameter to be considered for photopolymerization of the adhesive hydrogels below the tissue. As a consequence of light scattering by the tissue, the NIR coherent beam of light (square aperture) turns into an extended speckle pattern whose transverse area increases with respect to the thickness of the tissue. Therefore, the resulting illumination intensity decreases faster than the total transmission. Experimentally, we measured that the normalized intensity (which is the intensity at a given depth normalized by the intensity in absence of tissue) of 405 nm light is decreased by 99% at 200 μm tissue thickness and 99.9% at 400 μm thickness due to less transmission and larger speckle area as depicted in Figure 3c. The speckle area of tissue-transmitted NIR light, in the middle of a hydrogel sample, is smaller than that of the visible light, as NIR is less subject to scattering in the tissue than UV/blue light. In agreement with the literature, this proves the advantage of using NIR light, particularly for thick tissues (>200 μm). Figure 3a (right hand side) illustrates the transverse size of the beams (NIR and blue light) at the microscope objective's focal plane after propagating through 100, 200, and 300 μm tissue thicknesses. Blue light could not be detected after 500 μm tissue thickness. It should be noted that these measurements on light transmission are reported here for cartilage tissue (from bovine knee) that is relatively scattering compared to skin. We thus expect a different behavior for other biological tissues.

As stated above, upconversion of NIR into shorter wavelength light is crucial to initiate polymerization. We employed LAP, which requires UV light, to trigger polymerization. Subsequently, $NaYF_4$/Yb,Tm UCNPs were synthesized, according to the previously reported protocols[24,26] onto which LAP was attached for higher initiation efficiency and then added to the precursor of adhesive hydrogels. Transmission electron microscopy (TEM) analysis of UCNPs (ESI) confirmed the formation of core−shell particles where seed particles are of a smaller size (41.2 ± 2.78 nm) than core−shell (44.11 ± 3.65 nm) UNCP particles (Supporting Figure 4). Moreover, core−shell particles are hexagonal in shape, where seed particles are spherical in shape (Supporting Figure 5). Once LAP is coated onto UCNPs, the zeta (ζ) potential of UCNPs was reduced from 51.7 ± 11.4 to −1.3 ± 6.71 mV, which confirms the coating formation (Supporting Figure 6).

A precursor of the gelatin-based hydrogel (containing 15 wt % polymer content, with 15 mg/mL UCNPs and 0.2 wt % LAP, in a mold) was placed under the tissue and irradiated

https://doi.org/10.1021/acs.biomac.2c00811
Biomacromolecules 2022, 23, 5007−5017

with the 976 nm wavelength laser beam, at 0.7 W light power, and a beam waist of 19 μm focused into the precursor. Note that this is done on the same experimental apparatus as the one used to measure tissue optical properties in Figure 3. We observed cured hydrogels below the tissue of up to 300 μm thickness. No polymerization took place at larger thicknesses as the energy of transmitted light decreases with increasing tissue thickness. Nevertheless, we expect hydrogel polymerization through a larger cartilage thickness with UCNPs of higher upconversion efficiency.

After polymerization, we examined the compressive stiffness of cured adhesive hydrogels. As shown in Figure 4, the stiffness

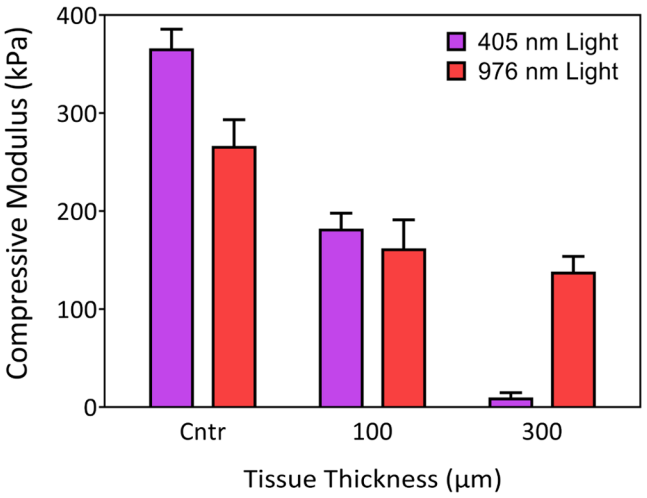

Figure 4. Mechanical properties of the polymerized hydrogel + UCNPs using 976 and 405 nm irradiation under different tissue thicknesses. Once a precursor of the hydrogel (containing 15 wt % polymer contents with 15 mg/mL UCNPs and 0.2 wt % LAP in a mold) was placed under the tissue; a laser beam of 976 nm wavelength, 19 μm of diameter, and 0.7 W power was used to irradiate the sample from the top for 10 min. Photopolymerization using 405 nm light was conducted on a conventional setup with a uniform illumination using a lamp (see the Methods Section).

of the hydrogel decreases with increasing tissue thickness. The control sample (without a tissue on the top) has a stiffness of 266.4 ± 26.5 kPa, whereas the hydrogel obtained below a 300 μm thick tissue exhibits a stiffness of 138.2 ± 15.5 kPa. As one would expect, this demonstrates that the higher the tissue thickness, the lower the NIR transmitted, which affects the upconverted fluorescence intensity and ultimately the polymerization kinetics. Lower fluorescence intensity results in less excited photoinitiators, which will affect the network formation from the polymer chains. Subsequently, this will produce a hydrogel with a mixture of oligomers and polymers with a low cross-linked density dictating the mechanical properties of cured hydrogels. To compare the proposed NIR system with conventional UV/blue photocuring methods, we also cross-link adhesive hydrogels using a 405 nm lamp with uniform illumination. These experiments are performed on a separate setup where the blue light illuminates the full gel to reproduce the common photocuring practice. Mechanical properties of these hydrogels are similar to UCNP-based hydrogels when cured below 100 μm tissue thickness; however, for thicker tissues, the polymerization is extremely weak, and the hydrogel remains in a liquid form. This confirms the performance of the NIR excitation we use with (1) a higher wavelength for higher transmission and (2) a focused beam to maximize the UV/blue light emission. Still, hydrogel gelation could not be seen after 500 μm tissue thickness, indicating the scattered property of tissue as well as the limited upconversion efficiency of UCNPs.

The conventional photopolymerization technique (using UV/blue light) is linear, where the whole samples are fully illuminated, and is simultaneously polymerized. However, this is not the case here when using a focused NIR light and UCNPs. Here, an NIR laser is focused right in the middle of a sample, from where the polymerization process is initiated (by UCNPs), Figure 1. This suggests that the polymerization took place first in the middle, and later the propagation follows across the sample. This hypothesis is further proved after increasing the NIR laser power and the concentration of UCNPs in hydrogel's precursors.

Owing to the versatility of the optical parameters and material composition, the mechanical properties of adhesive hydrogels can be tuned, such as by adjusting NIR laser power and the nanoparticle concentration. These changes should influence the adhesive as well as the mechanical performance of cured hydrogels. Keeping precursor composition (including 15 mg/mL of UCNPs and 15 wt % of polymer content) fixed, different laser powers were used to polymerize the adhesive hydrogels below the host layer. As depicted in Figure 5a,b, laser power indeed affects the properties of cured hydrogels. Power increase leads to higher adhesive and mechanical performance. We found that with 0.7 W laser power, the compressive modulus of the hydrogel (266.5 ± 26.6 kPa) is increased by 19.5%, whereas the adhesion strength (46.7 ± 4.5 kPa) is improved by 31.6%. However, with 0.9 W laser power, the compressive modulus (264.7 ± 40.4 kPa) and the adhesion strength of the hydrogel (44.5 ± 6.5 kPa) do not show a significant change. This suggests that UCNPs, at a specific concentration and laser power, receive sufficient transmitted energy from NIR light and reach a saturation level with blue light emission.

At constant laser power (0.5 W), the effect of the UNCP concentration on curing hydrogels is further evaluated. Three different concentrations, 10, 15, and 20 mg/mL are added to the precursor solution. As shown in Figure 5c,d, for the adhesive hydrogel cured with the highest UCNP concentration (20 mg/mL), the compressive modulus was increased by 94% and the adhesion strength by 101%, compared to the hydrogel with 10 mg/mL UCNPs. We believe that with higher particle concentration, upconversion of NIR into blue light should be higher and better distributed. This should enhance network formation efficiency and form the hydrogel of longer polymer chain length. It will readily improve the degree of cross-linking and polymer chain entanglements in the hydrogels, which exhibit improved mechanical properties.[28−30]

The obtained adhesive hydrogels, owing to the spatial shape of the NIR light (i.e., focused beam) for photocuring, present a gradient profile in mechanical properties. To demonstrate that the NIR-mediated photocuring of adhesive hydrogels is a nonlinear polymerization phenomenon, the mechanical property of cylindrical-shaped hydrogels with different UCNP concentrations is measured by nanoindentation at three different radial positions, *i.e.,* center, middle, and edge (Figure 6a). We found that in the central region (0.1 R, where laser beam is focused), no significant difference in the applied indentation force is observed. At a constant penetration depth (20 μm) of an indenter, the maximum indentation force is merely increased from 12.8 ± 1.4 to 14.4 ± 1.7 mN of

https://doi.org/10.1021/acs.biomac.2c00811
Biomacromolecules 2022, 23, 5007−5017

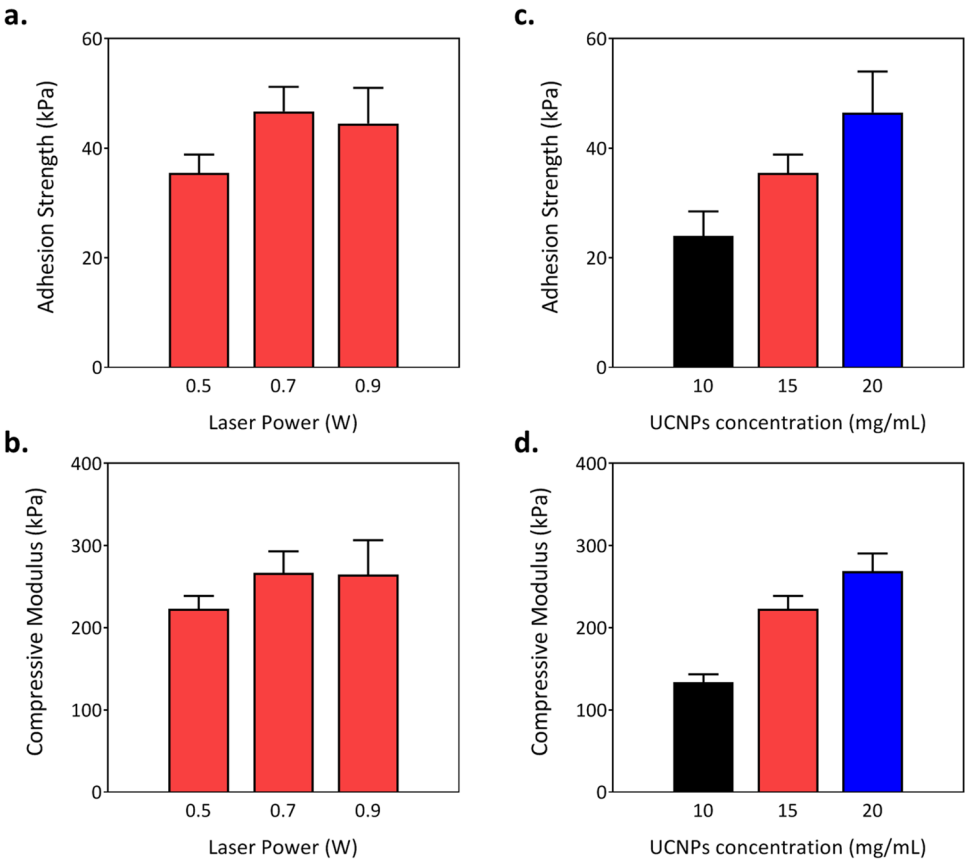

Figure 5. (a, b) Effect of NIR laser power on the compressive modulus and adhesion strength of cured hydrogels at 15 mg/mL UCNP concentration. (c, d) Effect of the UNCP concentration on the compressive modulus and adhesion strength at a laser power of 0.5 W (n = 3).

hydrogels with 10 to 20 mg/mL of UCNPs, respectively (Figure 6a,b). This observation clearly demonstrates that the UCNP concentration is not a limiting factor in the close vicinity of the laser beam. In other words, the maximum polymerization, allowed in this hydrogel system, has been reached in this region.

However, the effect of particle concentrations is significant in the middle and edge of the hydrogels. As exhibited in Figure 6b, at the edge of the cylindrical hydrogel sample (0.9 R), the recorded indentation force is 7.5 ± 1.6, 11.4 ± 1.5, and 13.5 ± 1.8 mN for hydrogels incorporated 10, 15, and 20 mg/mL of UCNPs, respectively. This confirms that the maximum indentation force increases with the particle concentration, revealing a better polymerization in this region which is strongly dependent upon the amount of emitted short-wavelength fluorescent light from UCNPs.

The effect of the UCNP concentration on bulk polymerization was also confirmed through image analysis under a Leica DM5500 upright microscope. Due to the multimode fibercoupled laser diode, the beam focused into the hydrogel has a speckle pattern, resulting in the inhomogeneity of 976 nm light. Brightspeckle grains have a high intensity, and therefore, they will produce a strong fluorescence signal that triggers the polymerization in a farther region quickly, forming the radiation lines (Figure 6c). We believe that the change in the refractive index, induced by the polymerization, is responsible for the formation of radiation lines. The influence of the UCNP concentration to the energy radiation throughout the sample, from the center to the edge, is evident. At a high UCNP concentration, blue light emission is strong enough to polymerize a cylindrical hydrogel with longer polymer chains and rigid characteristics. The polymerization creates clear radiation lines on the surface of the polymerized cylindrical hydrogel. When the UCNP concentration decreases, the (monomer) conversion is weaker and limited to form oligomers of GelMA, forming a rather smoother surface. This signifies that at a high UCNP concentration, a larger area around the illumination spot reaches the threshold energy for photoinitiator activation and consequently free radical polymerization. Therefore, the degree of cross-linking between polymer chains in respective hydrogels is greater. This is reflected further in the mechanical properties of the bulk hydrogel with different concentrations of UCNPs, as shown in Figure 5c,d. Moreover, the results, in Figure 6a−c, clearly demonstrates the gradient in mechanical properties using photopolymerization mediated by the NIR light beam. The mechanical response of the hydrogel with 20 mg/mL UCNP concentration is similar at different radial locations, indicating that there is a sufficient amount of emitted short-wavelength fluorescent light from UCNPs throughout the samples for initiating polymerization. Conversely, hydrogels with lower UCNP concentrations show a gradient mechanical response from the center to the edge. Larger regions can be fully polymerized by developing UCNPs with higher efficiency or illuminating for a longer time, resulting in more even distribution of mechanical properties.

Although demonstrated for the first time, there are still some limitations, which need to be addressed for further improvement of this approach. Owing to the low upconversion efficiency of UCNPs, high NIR laser power and particle

https://doi.org/10.1021/acs.biomac.2c00811
Biomacromolecules 2022, 23, 5007−5017

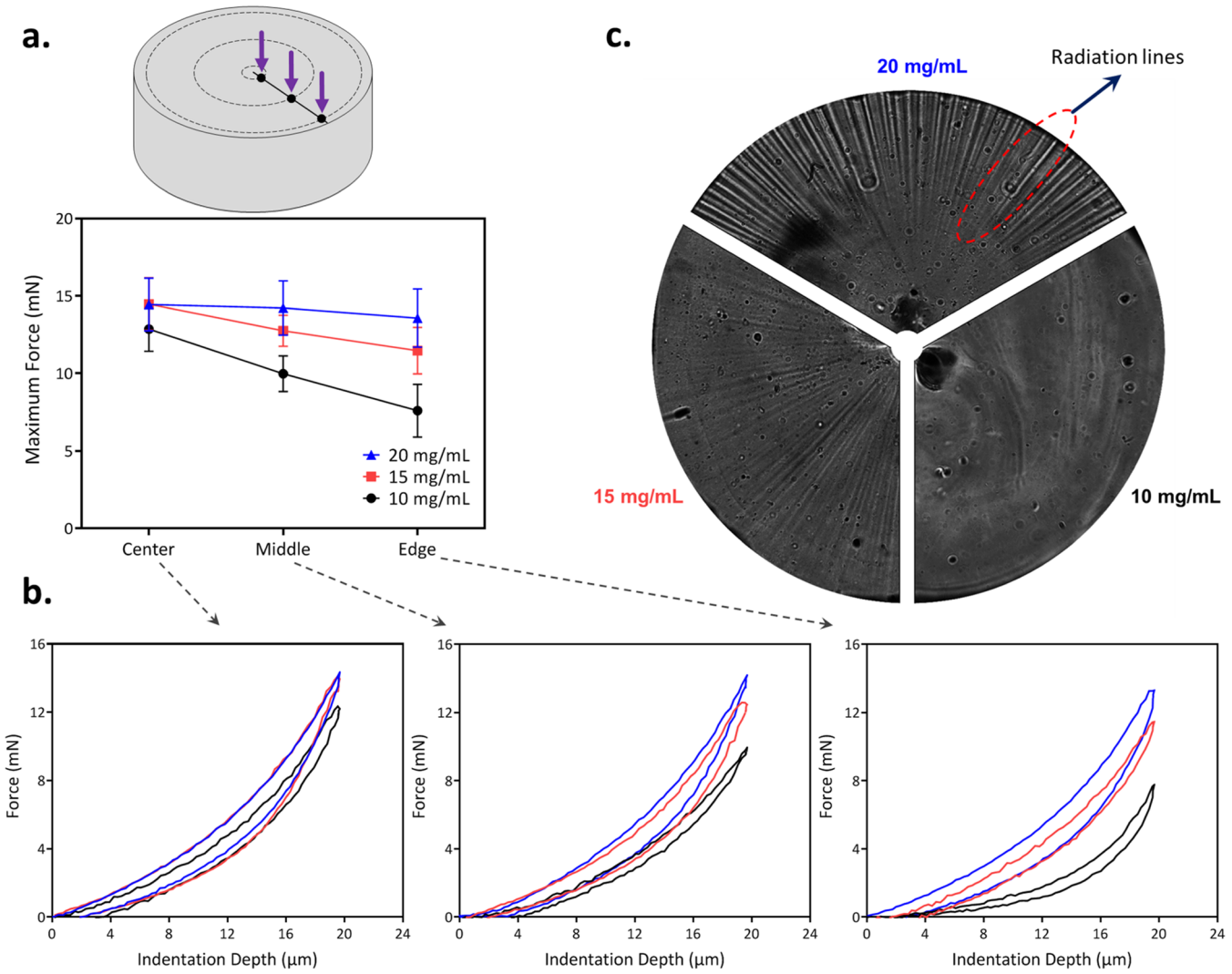

Figure 6. Effect of the UCNP concentration: (a) nanoindentation measurements and the obtained maximum indentation force at the radii of 0.1 *R*, 0.5 *R*, and 0.9 *R* from the cylinder axis (R = 2.5 mm, cylinder radius) and (b) representative force−displacement curves obtained during the indentation analysis. (c) The radiation lines generated by NIR laser and upconversion procedure from the center to the edge were imaged using a Leica DM5500 upright microscope.

concentrations were employed to initiate photopolymerization. However, improving the UCNP upconversion efficiency can be obtained by various techniques such as tailoring the local crystal field, dopant concentration, ratio of core/shell materials, suppression of surface-related deactivations, *etc.* Indeed, by optimizing the doping concentration and the size and structure of UCNPs, a higher upconversion efficiency at the UV/blue region that matches the absorption peak of the photoinitiator can be achieved, which will enable photopolymerization with clinically safe dose.[31−33] Moreover, further investigations are required to look beyond the LAP photoinitiator or develop photoinitiators that can trigger polymerization by low-energy photons.

CONCLUSIONS

We proposed a new method for curing the adhesive hydrogels below and inside biological tissues that could be an alternative noninvasive technique to treat injured soft tissues. As expected, we initially found that the transmission of NIR (976 nm) through various tissue thicknesses is much greater than 405 nm light. Transmitted NIR is then upconverted by UCNPs into lower wavelength blue light to trigger photopolymerization. Subsequently, the adhesive hydrogel is formed below the tissue. NIR laser power and particle concentrations were employed to tune the mechanical as well as adhesive properties of cured adhesive hydrogels. We found that the adhesive hydrogel cured with the highest UCNP concentration (20 mg/mL) showed up to 94 and 101% gain in compressive modulus and adhesion strength compared to a hydrogel with 10 mg/mL UCNPs, respectively. Interestingly, nanoindentation and microscopy analysis depicted the profile of the polymerized object and confirmed that curing adhesive hydrogels below the tissue, using NIR, is a nonlinear photopolymerization phenomenon. In fact, to reach such polymerization kinetics, we employed a radiation technique to polymerize the adhesive hydrogels below and inside the tissue by combining the local radiation of focused NIR and the bulk emission of blue light by UCNPs. Once, the sufficient upconversion efficiency of UCNPs in the blue/UV region, which matches the absorption peak of the photoinitiator, is achieved, that will pave the way for assembling the adhesive hydrogels through tissue. Hereafter, this technique can be used to reduce surgical

https://doi.org/10.1021/acs.biomac.2c00811
Biomacromolecules 2022, 23, 5007−5017

interventions and cause minor incisions. Thus, the tissue will be less damaged by the established surgical treatments.

■ ASSOCIATED CONTENT

Supporting Information

The Supporting Information is available free of charge at https://pubs.acs.org/doi/10.1021/acs.biomac.2c00811.

Spectra measurement (emission spectrum of UCNPs and the absorption spectrum of LAP); cytotoxicity analysis; TEM images on particle sizes confirming the core/shell structure; SEM images of the hydrogel confirming the particle distributions in it; analysis of gelatin chemical modification by NMR, and ζ-potential measurements (PDF)

■ AUTHOR INFORMATION

Corresponding Author

Dominique P. Pioletti − *Laboratory of Biomechanical Orthopaedics, Institute of Bioengineering, School of Engineering, EPFL, Lausanne 1015, Switzerland;* orcid.org/0000-0001-5535-5296; Email: dominique.pioletti@epfl.ch

Authors

Peyman Karami − *Laboratory of Biomechanical Orthopaedics, Institute of Bioengineering, School of Engineering, EPFL, Lausanne 1015, Switzerland;* orcid.org/0000-0003-1098-4296

Vijay Kumar Rana − *Laboratory of Biomechanical Orthopaedics, Institute of Bioengineering, School of Engineering, EPFL, Lausanne 1015, Switzerland;* orcid.org/0000-0001-7307-6653

Qianyi Zhang − *Laboratory of Applied Photonics Devices, Institute of Electrical and Micro Engineering, School of Engineering, EPFL, Lausanne 1015, Switzerland*

Antoine Boniface − *Laboratory of Applied Photonics Devices, Institute of Electrical and Micro Engineering, School of Engineering, EPFL, Lausanne 1015, Switzerland*

Yanheng Guo − *Laboratory of Biomechanical Orthopaedics, Institute of Bioengineering, School of Engineering, EPFL, Lausanne 1015, Switzerland;* orcid.org/0000-0002-3131-3283

Christophe Moser − *Laboratory of Applied Photonics Devices, Institute of Electrical and Micro Engineering, School of Engineering, EPFL, Lausanne 1015, Switzerland*

Complete contact information is available at: https://pubs.acs.org/10.1021/acs.biomac.2c00811

Author Contributions

§P.K., V.K.R., and Q.Z. contributed equally to this work.

Notes

The authors declare no competing financial interest.

■ ACKNOWLEDGMENTS

This work was supported by an SNF Grant #CRSIIS_189913 and by a grant from the eSeed Initiative at the EPFL School of Engineering. The authors thank Dr. Anna Loiudice of LNCE EPFL for her help with UCNP synthesis.

■ REFERENCES

(1) Kwon, H.; Brown, W. E.; Lee, C. A.; Wang, D.; Paschos, N.; Hu, J. C.; Athanasiou, K. A. Surgical and tissue engineering strategies for articular cartilage and meniscus repair. *Nat. Rev. Rheumatol.* **2019**, *15*, 550−570.

(2) Hong, Y.; Zhou, F.; Hua, Y.; Zhang, X.; Ni, C.; Pan, D.; Zhang, Y.; Jiang, D.; Yang, L.; Lin, Q.; Zou, Y.; et al. A strongly adhesive hemostatic hydrogel for the repair of arterial and heart bleeds. *Nat. Commun.* **2019**, *10*, No. 2060.

(3) Xue, B.; Gu, J.; Li, L.; Yu, W.; Yin, S.; Qin, M.; Jiang, Q.; Wang, W.; Cao, Y. Hydrogel tapes for fault-tolerant strong wet adhesion. *Nat. Commun.* **2021**, *12*, No. 7156.

(4) Bernal, P. N.; Delrot, P.; Loterie, D.; Li, Y.; Malda, J.; Moser, C.; Levato, R. Volumetric bioprinting of complex living-tissue constructs within seconds. *Adv. Mater.* **2019**, *31*, No. 1904209.

(5) Rana, V. K.; Tabet, A.; Vigil, J. A.; Balzer, C. J.; Narkevicius, A.; Finlay, J.; Hallou, C.; Rowitch, D. H.; Bulstrode, H.; Scherman, O. A. Cucurbit [8] uril-derived graphene hydrogels. *ACS Macro Lett.* **2019**, *8*, 1629−1634.

(6) Nasrollahzadeh, N.; Karami, P.; Pioletti, D. P. Control of dissipation sources: a central aspect for enhancing the mechanical and mechanobiological performances of hydrogels. *ACS Appl. Mater. Interfaces* **2019**, *11*, 39662−39671.

(7) Karami, P.; Nasrollahzadeh, N.; Wyss, C.; O'Sullivan, A.; Broome, M.; Procter, P.; Bourban, P. E.; Moser, C.; Pioletti, D. P. An Intrinsically-Adhesive Family of Injectable and Photo-Curable Hydrogels with Functional Physicochemical Performance for Regenerative Medicine. *Macromol. Rapid Commun.* **2021**, *42*, No. 2000660.

(8) Wyss, C. S.; Karami, P.; Demongeot, A.; Bourban, P. E.; Pioletti, D. P. Silk granular hydrogels self-reinforced with regenerated silk fibroin fibers. *Soft Matter* **2021**, *17*, 7038−7046.

(9) Lee, G. H.; Moon, H.; Kim, H.; Lee, G. H.; Kwon, W.; Yoo, S.; Myung, D.; Yun, S. H.; Bao, Z.; Hahn, S. K. Multifunctional materials for implantable and wearable photonic healthcare devices. *Nat. Rev. Mater.* **2020**, *5*, 149−165.

(10) Bagheri, A.; Jin, J. Photopolymerization in 3D printing. *ACS Appl. Polym. Mater.* **2019**, *1*, 593−611.

(11) Sandell, J. L.; Zhu, T. C. A review of in-vivo optical properties of human tissues and its impact on PDT. *J. Biophotonics* **2011**, *4*, 773−787.

(12) Jacques, S. L. Optical properties of biological tissues: a review. *Phys. Med. Biol.* **2013**, *58*, R37−R61.

(13) Wang, M.; Abbineni, G.; Clevenger, A.; Mao, C.; Xu, S. Upconversion nanoparticles: synthesis, surface modification and biological applications. *Nanomedicine* **2011**, *7*, 710−729.

(14) Chen, Z.; Wang, X.; Li, S.; Liu, S.; Miao, H.; Wu, S. Near-Infrared Light Driven Photopolymerization Based On Photon Upconversion. *ChemPhotoChem* **2019**, *3*, 1077−1083.

(15) Liu, X.; Chen, H.; Wang, Y.; Si, Y.; Zhang, H.; Li, X.; Zhang, Z.; Yan, B.; Jiang, S.; Wang, F.; Weng, S.; et al. Near-infrared manipulation of multiple neuronal populations via trichromatic upconversion. *Nat. Commun.* **2021**, *12*, No. 5662.

(16) Yan, B.; Boyer, J. C.; Habault, D.; Branda, N. R.; Zhao, Y. Near infrared light triggered release of biomacromolecules from hydrogels loaded with upconversion nanoparticles. *J. Am. Chem. Soc.* **2012**, *134*, 16558−16561.

(17) Sordillo, L. A.; Pu, Y.; Pratavieira, S.; Budansky, Y.; Alfano, R. R. Deep optical imaging of tissue using the second and third near-infrared spectral windows. *J. Biomed. Opt.* **2014**, *19*, No. 056004.

(18) Sarder, P.; Yazdanfar, S.; Akers, W. J.; Tang, R.; Sudlow, G. P.; Egbulefu, C.; Achilefu, S. All-near-infrared multiphoton microscopy interrogates intact tissues at deeper imaging depths than conventional single-and two-photon near-infrared excitation microscopes. *J. Biomed. Opt.* **2013**, *18*, No. 106012.

(19) Chen, E. Y.; Milleville, C.; Zide, J. M. O.; Doty, M. F.; Zhang, J. Upconversion of low-energy photons in semiconductor nanostructures for solar energy harvesting. *MRS Energy Sustainability* **2018**, *5*, No. 14.

(20) Demina, P.; Arkharova, N.; Asharchuk, I.; Khaydukov, K.; Karimov, D.; Rocheva, V.; Nechaev, A.; Grigoriev, Y.; Generalova, A.; Khaydukov, E. Polymerization assisted by upconversion nanoparticles under NIR light. *Molecules* **2019**, *24*, No. 2476.

(21) Chen, G.; Qiu, H.; Prasad, P. N.; Chen, X. Upconversion nanoparticles: design, nanochemistry, and applications in theranostics. *Chem. Rev.* **2014**, *114*, 5161−5214.
(22) Huang, L.; Le, T.; Huang, K.; Han, G. Enzymatic enhancing of triplet−triplet annihilation upconversion by breaking oxygen quenching for background-free biological sensing. *Nat. Commun.* **2021**, *12*, No. 1898.
(23) Zhu, X.; Su, Q.; Feng, W.; Li, F. Anti-Stokes shift luminescent materials for bio-applications. *Chem. Soc. Rev.* **2017**, *46*, 1025−1039.
(24) Chen, Y.; Zhang, J.; Liu, X.; Wang, S.; Tao, J.; Huang, Y.; Wu, W.; Li, Y.; Zhou, K.; Wei, X.; Chen, S.; et al. Noninvasive in vivo 3D bioprinting. *Sci. Adv.* **2020**, *6*, No. eaba7406.
(25) Wang, F.; Han, Y.; Lim, C. S.; Lu, Y.; Wang, J.; Xu, J.; Chen, H.; Zhang, C.; Hong, M.; Liu, X. Simultaneous phase and size control of upconversion nanocrystals through lanthanide doping. *Nature* **2010**, *463*, 1061−1065.
(26) Chen, S.; Weitemier, A. Z.; Zeng, X.; He, L.; Wang, X.; Tao, Y.; Huang, A. J.; Hashimotodani, Y.; Kano, M.; Iwasaki, H.; Parajuli, L. K. Near-infrared deep brain stimulation via upconversion nanoparticle−mediated optogenetics. *Science* **2018**, *359*, 679−684.
(27) You, S.; Li, J.; Zhu, W.; Yu, C.; Mei, D.; Chen, S. Nanoscale 3D printing of hydrogels for cellular tissue engineering. *J. Mater. Chem. B* **2018**, *6*, 2187−2197.
(28) Fu, J. Strong and tough hydrogels crosslinked by multifunctional polymer colloids. *J. Polym. Sci., Part B: Polym. Phys.* **2018**, *56*, 1336−1350.
(29) Sikdar, P.; Uddin, M. M.; Dip, T. M.; Islam, S.; Hoque, M. S.; Dhar, A. K.; Wu, S. Recent advances in the synthesis of smart hydrogels. *Mater. Adv.* **2021**, *2*, 4532−4573.
(30) Karami, P.; Wyss, C. S.; Khoushabi, A.; Schmocker, A.; Broome, M.; Moser, C.; Bourban, P. E.; Pioletti, D. P. Composite double-network hydrogels to improve adhesion on biological surfaces. *ACS Appl. Mater. Interfaces* **2018**, *10*, 38692−38699.
(31) Ai, F.; Ju, Q.; Zhang, X.; Chen, X.; Wang, F.; Zhu, G. A core-shell-shell nanoplatform upconverting near-infrared light at 808 nm for luminescence imaging and photodynamic therapy of cancer. *Sci. Rep.* **2015**, *5*, No. 10785.
(32) Zhou, Z.; Kong, B.; Yu, C.; Shi, X.; Wang, M.; Liu, W.; Sun, Y.; Zhang, Y.; Yang, H.; Yang, S. Tungsten oxide nanorods: an efficient nanoplatform for tumor CT imaging and photothermal therapy. *Sci. Rep.* **2015**, *4*, No. 3653.
(33) Liu, T. M.; Conde, J.; Lipiński, T.; Bednarkiewicz, A.; Huang, C. C. Revisiting the classification of NIR-absorbing/emitting nanomaterials for in vivo bioapplications. *NPG Asia Mater.* **2016**, *8*, No. e295.

https://doi.org/10.1021/acs.biomac.2c00811
Biomacromolecules 2022, 23, 5007−5017